**CSIRO** PUBLISHING

*International Journal of Wildland Fire* **2020**, *29*, 995–1008
https://doi.org/10.1071/WF19177

# A method for creating a burn severity atlas: an example from Alberta, Canada

*Ellen Whitman* [A,D], *Marc-André Parisien* [A], *Lisa M. Holsinger* [B], *Jane Park* [C] and *Sean A. Parks* [B]

[A]Natural Resources Canada, Canadian Forest Service, Northern Forestry Centre, 5320 122nd Street NW, Edmonton, AB T6H 3S5, Canada.
[B]USDA Forest Service, Aldo Leopold Wilderness Research Institute, 790 E Beckwith Avenue, Missoula, MT 59801, USA.
[C]Parks Canada Agency, Banff Field Unit, PO Box 900, Banff, AB T1L 1K2, Canada.
[D]Corresponding author. Email: ellen.whitman@canada.ca

**Abstract.** Wildland fires are globally widespread, constituting the primary forest disturbance in many ecosystems. Burn severity (fire-induced change to vegetation and soils) has short-term impacts on erosion and post-fire environments, and persistent effects on forest regeneration, making burn severity data important for managers and scientists. Analysts can create atlases of historical and recent burn severity, represented by changes in surface reflectance following fire, using satellite imagery and fire perimeters. Burn severity atlas production has been limited by diverse constraints outside the US. We demonstrate the development and validation of a burn severity atlas using the Google Earth Engine platform and image catalogue. We automated mapping of three burn severity metrics using mean compositing (averaging reflectance values) of pixels for all large (≥200 ha) fires in Alberta, Canada. We share the resulting atlas and code. We compared burn severity datasets produced using mean compositing with data from paired images (one pre- and post-fire image). There was no meaningful difference in model correspondence to field data between the two approaches, but mean compositing saved time and increased the area mapped. This approach could be applied and tested worldwide, and is ideal for regions with small staffs and budgets, and areas with frequent cloud.

**Additional keywords:** Composite Burn Index, fire atlas, fire mapping, fire severity, Google Earth Engine.

Received 23 October 2019, accepted 27 July 2020, published online 25 August 2020

## Introduction

Wildland fires are widespread across the globe, occurring wherever adequate fuels and climate conditions that allow combustion coincide (Krawchuk *et al.* 2009). When forest fires occur, varying fire intensity may cause mortality of mature trees and combustion of organic matter, including soils, coarse woody debris, and in the case of crown fires, cones and foliage. The range of biomass loss and subsequent ecological outcomes resulting from combustion are often described as burn severity (Morgan *et al.* 2014). Variability in burn severity structures landscape patterns, influences ecosystem spatial heterogeneity from landscape to stand levels and influences patterns of post-fire forest recovery in terms of both species compositions and forest structure (Turner *et al.* 1999; Schoennagel *et al.* 2008). Because burn severity is a key driver of landscape patterns and processes in forested ecosystems, spatially explicit burn severity data are extremely useful for scientific research, as well as for post-fire management of risk to watersheds, forest salvage and long-term forest recovery (Morgan *et al.* 2014). Burn severity can be mapped by differencing pre- and post-fire near-infrared (NIR) and short-wave infrared (SWIR) reflectance from multispectral imagery, thereby characterising fire-induced changes to vegetation and soils (Key and Benson 2006; Harvey *et al.* 2019). Several remotely sensed multispectral burn severity metrics have been developed, including the differenced Normalized Burn Ratio (dNBR; Key and Benson 2006), Relativized dNBR (RdNBR; Miller and Thode 2007) and the Relativized Burn Ratio (RBR; Parks *et al.* 2014*a*).

The composite burn index (CBI) is a field-measured burn severity index developed and used in the United States (Key and Benson 2006) and now applied in Europe and Canada (e.g. Hall *et al.* 2008; De Santis and Chuvieco 2009). CBI characterises the magnitude of fire effects summarised across all forest strata (surface to crown) on a continuous scale. CBI encompasses combustion of both live and dead organic matter, fire effects on soils, and post-fire recovery of native and invasive plants, thereby providing a measure of the ecological effects of fire (i.e. the burn severity) at a given site (Key and Benson 2006). Remotely sensed multispectral burn severity metrics often exhibit a strong relationship with the CBI, thereby supporting their use as a measure of severity across fires and forested landscapes (Key and Benson 2006; Morgan *et al.* 2014). Although CBI is not ideally suited to represent all ecological impacts from wildfire that are of research or management interest (French *et al.* 2008), other field-measured severity indices also correspond well to remotely sensed severity metrics (Reilly *et al.* 2017; Whitman *et al.* 2018*a*; Harvey *et al.* 2019).

The Landsat satellite series image catalogue is widely used for analyses of burn severity owing to the extensive historical record of 30-m resolution multispectral imagery (1984–present), which enables the development of multidecadal atlases of fire history and severity. One example of such an atlas is the Monitoring Trends in Burn Severity (MTBS) program in the United States, which distributes Landsat-derived burn severity maps for all large wildfires in the United States and Puerto Rico since 1984 (Eidenshink *et al.* 2007; US Geological Survey, USDA Forest Service and USDI 2019). Despite the utility of burn severity data for both the research and management communities and the proliferation of remotely sensed imagery, the production and use of comprehensive fire severity atlases are uncommon outside the US (Parks *et al.* 2018). In Canada, for example, past production of severity maps was conducted in a piecemeal fashion for small numbers of fires in specific areas of interest (e.g. Soverel *et al.* 2010; Whitman *et al.* 2015; San-Miguel *et al.* 2016; Boucher *et al.* 2017; Whitman *et al.* 2018*a*; but see San-Miguel *et al.* 2019). This is likely owing to the time-consuming nature of selecting paired images (one pre-fire and one post-fire) for each fire of interest, without the dedicated support of a public program for this purpose.

The advent of cloud computing and imagery compositing approaches have substantially reduced the effort and time required to develop atlases of remotely sensed severity indices. With the increasingly common use of pixel-level analyses for remote sensing applications, analyst selection of paired images for each fire (a time-consuming process requiring careful attention) may no longer be necessary. Furthermore, mean or median compositing of pixels (averaging multiple reflectance values for a single pixel across a prespecified date range) allows researchers to create comprehensive severity maps in areas with relatively few cloud-free images without missing fire events, an outcome that is possible using best-pixel (single reflectance value per pixel per year) composites (White *et al.* 2014). Although the processing power required for such pixel-level analyses was limiting in the past, cloud-computing platforms such as Google Earth Engine (GEE) have made such methods broadly accessible, and allow users to automate map-making. GEE also acts as an image catalogue, compiling and integrating temporally extensive imagery and products from diverse sources and sensors (e.g. the entire Landsat archive), thereby providing access to datasets of sizes prohibitively large for personal computing. In regions with accurate and comprehensive fire perimeter data, such as Canada, barriers to the production and subsequent analysis of burn severity maps are now minimal (Parks *et al.* 2018).

Our objectives for the present work were: (1) to demonstrate the semi-automated production a comprehensive fire severity atlas using mean compositing in GEE; (2) to compare the error and fit of models of burn severity fitted to severity metrics produced using paired images and mean compositing in GEE for 11 fires with field-measured CBI burn severity data; and (3) to characterise the relative area mapped using the two methods. The code used to produce this atlas is available for use at the following link: http://tidy.ws/4nkdMU (accessed 5 August 2020). The resulting fire severity atlas is also available for download upon request.

### *Study area*

This study examines the forested area of the province of Alberta and adjacent national parks (Fig. 1). Boreal forest covers much of this landscape, extending from the northern boundary of the study area to central Alberta, where the forest transitions into aspen parkland. The central south-eastern portion of Alberta consists of open prairie and agricultural land, and was not analysed for this research. The Rocky Mountains make up the south-western border of the province. These mountainous areas support montane and subalpine forests, which transition into foothills to the east where the montane meets the boreal and prairie ecoregions (Fig. 1).

Conifer tree species are dominant in forests throughout the study area. The boreal forest is characterised by black spruce (*Picea mariana* (Mill.) Britton, Sterns and Poggenburgh), jack pine (*Pinus banksiana* Lamb.) and white spruce (*Picea glauca* (Moench) Voss), with a broadleaf component from species such as trembling aspen (*Populus tremuloides* Michx.), balsam poplar (*Populus balsamifera* L.) and paper birch (*Betula papyrifera* Marshall). The dominant tree species in montane and subalpine forests are Englemann spruce (*Picea englemannii* Englemann), subalpine fir (*Abies lasiocarpa* (Hook.) Nuttall), Douglas-fir (*Pseudotsuga menziesii* (Mirbel) Franco), lodgepole pine (*Pinus contorta* var. *latifolia* Englemann) and trembling aspen.

Fire severity is substantially linked to pre-fire fuel structure and composition (Whitman *et al.* 2018*a*; Skowronski *et al.* 2020). Generally, these conifer-dominated forests provide vertically and horizontally continuous fuel for fires from the forest surface into the crown of trees, often allowing severe and extensive continuous crown fire in both boreal and cordillera regions. Fuels with a broadleaf component are unlikely to burn as crown fires, and burn less severely (Forestry Canada Fire Danger Group 1992; Tymstra *et al.* 2005; Whitman *et al.* 2018*a*). Within the cordillera ecoregion, montane forests have a more open forest structure in warm, dry, valley bottoms and where fire was historically more frequent and fire seasons are longer, creating a fuel structure promoting moderate- or mixed-severity fire, whereas higher-elevation subalpine forest fire regimes may be similar to those of the boreal, and are disposed to infrequent stand-replacing fire (DeLong and Meidinger 2003; Rogeau *et al.* 2004; Tymstra *et al.* 2005).

Wildfire is an extensive stand-replacing disturbance in Canadian forests, burning an average of 1.96 Mha annually (1959–2015). The majority of these fires occur in boreal forests (Stocks *et al.* 2002; Hanes *et al.* 2019). Wildfire activity and fire season lengths have significantly increased in western Canada since the 1960s, and an extensive area of the western Canadian landscape has burned since fire activity has been closely monitored (Hanes *et al.* 2019). Although the fire regime in boreal forests is generally characterised as stand-replacing (i.e. lethal to trees), there is substantial variability in burn severity and resulting ecological outcomes (Hall *et al.* 2008; Whitman

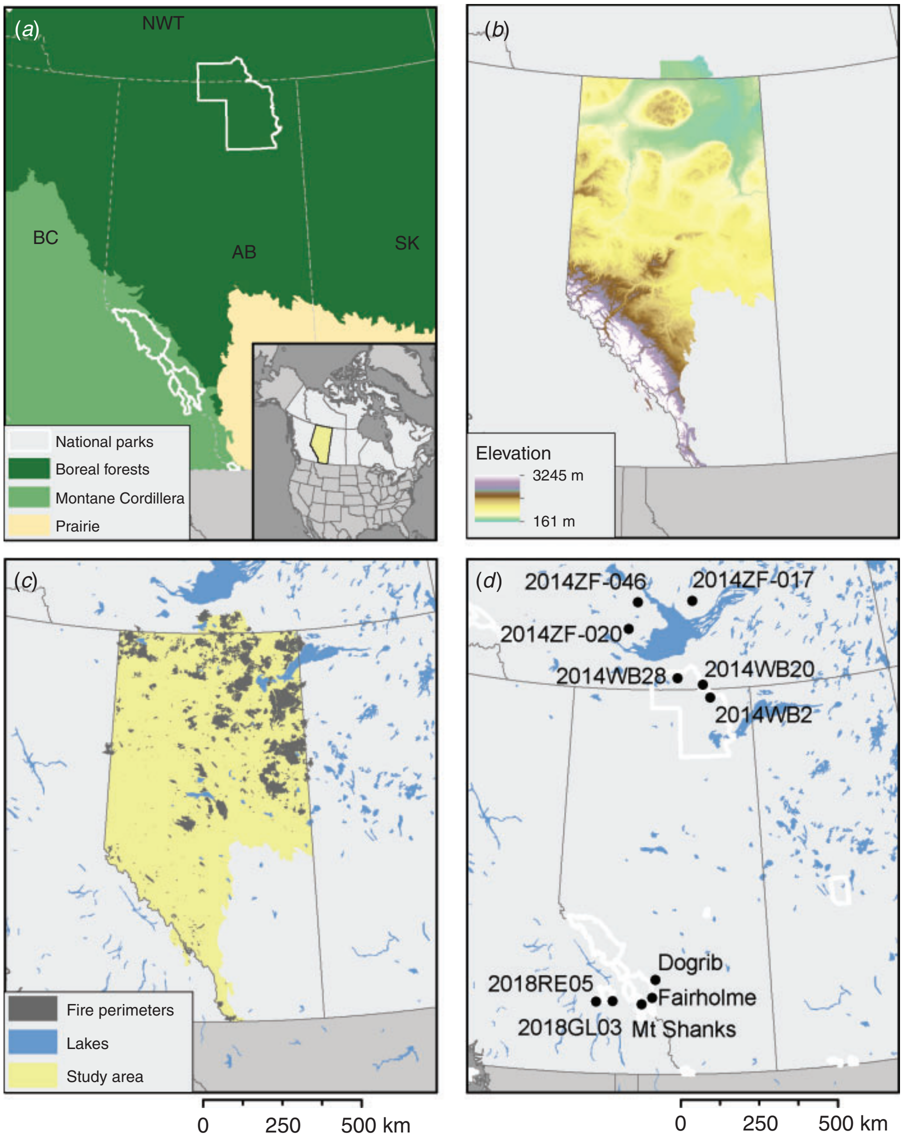


**Fig. 1.** Wildfires with field data used for model validation, and geography and environment of focal study area. (*a*) Ecozones generalised derived from the Ecological Framework of Canada (ESWG 1995) and nearby national parks included in study area, as well as the location of Alberta in North America; (*b*) elevation within the study area (Natural Resources Canada 2011); (*c*) perimeters of large (≥200 ha) wildfires (1985–2015) within the study area used to generate the fire severity atlas; and (*d*) 11 wildfires in British Columbia, Alberta and the Northwest Territories with field Composite Burn Index (CBI) data used in model validation.

*et al.* 2018*a*, 2018*b*). Large, lightning-ignited fires (≥200 ha) contribute the majority of area burned, with fire sizes being larger in the boreal zone than in the montane and foothills. (Stocks *et al.* 2002; Tymstra *et al.* 2005; Hanes *et al.* 2019). Wildfires typically occur in the study area between May and August, with the majority of ignitions happening in May and June in the boreal region, and in July and August in the montane cordillera (Tymstra *et al.* 2005). Fires in these ecosystems are both natural and human-caused, although there is a distinct lightning shadow where lightning-caused ignitions do not occur on the eastern slopes of the Rocky Mountains (Wierzchowski *et al.* 2002).

## Methods

### *Wildfire database*

We selected all fires ≥200 ha in size recorded in the Canadian National Fire Database (CNFDB; Natural Resources Canada 2019) that occurred between 1985 and 2018 within the study area (Fig. 1). We supplemented the CNFDB with fire perimeters produced for the National Burned Area Composite (NBAC) product (Hall *et al.* 2020) when the data quality of perimeters was superior to the corresponding fire in the CNFDB (provided by firefighting agencies), such as when fires crossed management borders, or when fires were missing from agency data. We

**Table 1. Unique identifiers for wildfires (Fire ID) and associated characteristics of 11 fires with field-measured Composite Burn Index (CBI) data, and analyst-selected pre-fire and post-fire paired Landsat scenes used for analysis**

BANP, Banff National Park; GLNP, Glacier National Park; KONP, Kootenay National Park; RENP, Mount Revelstoke National Park; WBNP, Wood Buffalo National Park

| Fire ID | Region and fire agency | Year | Size ($ha^{-1}$) | Number of CBI plots | Pre-fire Landsat scene | Post-fire Landsat scene |
|---|---|---|---|---|---|---|
| RWF085 | AB | 2001 | 10232 | 50 | LT50430241998218PAC03 | LT50430242002229LGS01 |
| 01KO012 | BC – KONP | 2001 | 3261 | 8 | LT50430251997231PAC03 | LT50430252002229LGS01 |
| 2003BA001 | AB – BANP | 2003 | 3615 | 195 | LT50420242001171XXX02 | LT50430242004171PAC02 |
| 2014ZF-017 | NWT | 2014 | 463650 | 5 | LC80450162014164LGN01 | LC80460162015174LGN01<br>LC80440162015176LGN03 |
| 2014ZF-020 | NWT | 2014 | 753429 | 15 | LC80480172013150LGN01 | LC80480172015140LGN01 |
| 2014ZF-046 | NWT | 2014 | 110144 | 21 | LC80480162013150LGN01 | LC80470162015149LGN02 |
| 2014WB2 | AB-WBNP | 2014 | 35470 | 9 | LT50440182011165PAC02 | LC80440182015176LGN03 |
| 2014WB20 | NWT-WBNP | 2014 | 11181 | 3 | LC80450182014164LGN01 | LC80440182015176LGN03 |
| 2014WB28 | NWT-WBNP | 2014 | 61227 | 10 | LC80450182014164LGN01 | LC80460182015174LGN01 |
| 2018RE05 | BC-RENP | 2018 | 260 | 22 | LC80440252017213LGN00 | LC80440252019203LGN00 |
| 2018GL03 | BC-GLNP | 2018 | 2799 | 86 | LC80440242016211LGN01 | LC80440242019219LGN00 |

filled 'doughnut hole' unburned islands and waterbodies that had been excluded by the agencies to produce consistent polygon perimeters with no inner holes in order to produce raster maps of burn severity that included values for unburned residuals. This resulted in a set of 796 fires for mapping in GEE. We mapped five additional fires that fell outside the study area (in the Northwest Territories, and Glacier and Mount Revelstoke National Parks; Fig. 1 and Table 1) because field-measured burn severity data (CBI) were available for calibration and validation (dataset described in Whitman *et al.* 2018*a*; Parks Canada Agency, unpublished data).

### *Remote sensing of burn severity*

Using GEE, we calculated the dNBR (Eqns 1, 2), RdNBR (Eqn 3) and RBR (Eqn 4) for each fire using Landsat imagery corrected to surface reflectance (http://tidy.ws/amjdCv; accessed 5 August 2020). We used the NIR and SWIR bands from Landsat 4–5 (Thematic Mapper (TM)) and Landsat-7 (Enhanced Thematic Mapper (ETM)+). We used the NIR and SWIR2 bands from Landsat-8 (Operational Land Imager (OLI)), as the wavelengths of these bands are the most similar to those of the earlier two Landsat satellites. Generally, we followed the procedure described by Parks *et al.* (2018) to create continuous pre-fire and post-fire imagery for analysis. Specifically, we used mean compositing (averaging) of the reflectance values of pixels from the year prior, and year after (one complete growing season) each fire using an 'extended assessment' approach to mapping burn severity (Key and Benson 2006). We used all cloud- and smoke-free pixels acquired from 1 June (Julian day 152) to 31 August (Julian day 243) to create mean composite pixel reflectance values. This window was selected to reflect local phenology, reflecting a time period during which live deciduous trees and shrubs should have leafed out. If individual pixels within a fire perimeter had one or zero cloud-free pixels in the year before the fire, we extended the window for selection of pixels for severity mapping stepwise (1 year at a time) up to 5 years per pixel, until all pixels had cloud-free pre-fire imagery. We used the same process to extend the post-fire imagery window for up to a maximum of 2 years post fire, when necessary. We used this shorter window for post-fire pixels to preserve the spectral response of wildfire impacts that could be affected by vegetation regrowth. We calculated dNBR using an 'offset', where dNBR values were adjusted based on the average dNBR value of unburned pixels in a 180-m buffer outside the fire perimeter (Key and Benson 2006). As RdNBR and RBR are relativised transformations of dNBR, the offset is carried forward in these metrics.

For a comparison with mean composited burn severity maps, we also selected paired pre- and post-fire Landsat scenes for 11 fires for which there were field-measured CBI data available (Table 1) and produced all burn severity metrics from surface reflectance imagery (LEDAPS pre-processing (Landsat 4–7), Masek *et al.* 2006; LaSRC pre-processing (Landsat 8), Vermote *et al.* 2016).

$$\mathrm{NBR} = \frac{\mathrm{NIR} - \mathrm{SWIR}}{\mathrm{NIR} + \mathrm{SWIR}} \tag{1}$$

$$\mathrm{dNBR} = \left(\left(\mathrm{NBR}_{pre-fire} - \mathrm{NBR}_{post-fire}\right) \times 1000\right) - \mathrm{dNBR}_{offset} \tag{2}$$

$$\mathrm{RdNBR} = \frac{\mathrm{dNBR}}{\left|\left(\mathrm{NBR}_{pre-fire}\right)\right|^{0.5}} \tag{3}$$

$$\mathrm{RBR} = \frac{\mathrm{dNBR}}{\left|\left(\mathrm{NBR}_{pre-fire} + 1.001\right)\right|} \tag{4}$$

### *Comparison of burn severity remote sensing methods*

We compared the ability of the paired-image burn severity metrics to represent field observations of burn severity with those calculated using mean compositing in GEE with non-linear least-squares (NLS) regression. We fitted NLS models with a saturated growth form, relating field measurements of CBI (range from 0 (unburned) to 3 (severely burned)) to each remotely sensed burn severity metric and data source. We weighted the importance of field observations by the value of

**Table 2. Model fit (pseudo-$R^2$), error and bias estimates of model standard error (S), root-mean-square error (RMSE) and mean absolute error (MAE) for non-linear least-squares saturated growth models predicting Composite Burn Index (CBI) from burn severity metrics of the differenced Normalized Burn Ratio (dNBR), Relativized dNBR (RdNBR) and Relativized Burn Ratio (RBR) produced from paired images and mean compositing**

Model statistics were produced using cross-validation (CV) with models fitted using nine fires and tested on the remaining two fires with 1000 repeats

| Remotely sensed severity metric and method | CV $R^2$ | CV RMSE | CV MAE |
|---|---|---|---|
| $dNBR_{paired}$ | 0.71 | 0.52 | 0.40 |
| $dNBR_{mean\ composite}$ | 0.69 | 0.60 | 0.46 |
| $RdNBR_{paired}$ | 0.75 | 0.50 | 0.39 |
| $RdNBR_{mean\ composite}$ | 0.70 | 0.58 | 0.45 |
| $RBR_{paired}$ | 0.73 | 0.50 | 0.38 |
| $RBR_{mean\ composite}$ | 0.71 | 0.57 | 0.45 |

CBI, assigning high importance to very-high-severity CBI values in order to produce model estimations that more appropriately captured the range and extremes of possible CBI values. Model predictions were truncated to range between 0 and 3 in order to remove predicted CBI values outside the logical range. We assessed model quality by comparing the cross-validated (CV) coefficient of determination (pseudo-$R^2$, calculated using linear regression between observed and predicted CBI), as well as the model standard error (S), root-mean-square error (RMSE) and mean absolute error (MAE; a measure of bias). To accurately characterise model fits, we cross-validated with CBI plots from a random sample of 80% of fires ($n = 9$) as partitioned for model training, and CBI from 20% of fires ($n = 2$) used for testing of that model, repeated 1000 times.

CBI and burn severity maps are often broken into categories of 'unchanged' (no fire, or extremely limited impact on vegetation and soil), 'low' severity (surface fire with limited charring, some residual understorey vegetation may remain in places), 'moderate' severity (mixed overstorey tree mortality, more extensive understorey charring and combustion), and 'high' severity (near-complete or 100% overstorey mortality, crown involvement in the fire, and extensively charred or entirely combusted organic soils and debris; Key and Benson 2006). Using the NLS models created for cross-validation, we also estimated 1000 threshold values per severity metric and method, for breakpoints between high and moderate severity (CBI = 2.25), moderate and low severity (CBI = 1.5) and low-severity fire and unchanged areas (CBI = 0.1) using inverse estimation (Greenwell and Schubert Kabban 2014). We then compared the bootstrapped 95% confidence intervals and mean threshold values for each method and severity metric, computed from 1000 bootstrapped resamples.

To describe the relationships between severity maps generated using paired images and mean compositing in GEE, we randomly sampled 0.01% of pixels from each of 11 fires with field data and conducted CV Spearman correlation tests with 1000 repeats ($P$ values combined using harmonic means; Wilson 2019). A 0.01% sample was used to reduce the effect of spatial autocorrelation (i.e. pseudo-replication) associated with satellite-derived burn severity datasets. Finally, we compared the area mapped within fire perimeters using the two methods (paired imagery and mean compositing). To examine what proportion of pixels used imagery from beyond the ideal image selection window (1 year pre-fire, 1 year post-fire) in the mean-composited maps, we classified pixels as: (1) having pre-fire and post-fire imagery from the years immediately before and after the fire; (2) having either pre-fire or post-fire imagery from 2 years before or after the fire; or (3) having pixel values where the pre-fire imagery was from more than 2 years before the fire, or where both pre-fire and post-fire imagery were from 2 years before and after the fire. We also compared the proportion of pixels with no data or 'NA' values between paired and composite maps and characterised the gain in mapped area from extending the image selection window and using mean compositing.

## Results

Field measurements of CBI were strongly related to all three remotely sensed burn severity metrics and were well represented by similar saturated growth model forms (Table 2 and Fig. 2). No single metric substantially outperformed the others, although both relativised metrics had marginally lower model error (Table 2). The cross-validated pseudo-$R^2$ of predicted *v.* observed CBI ranged from 0.69 to 0.75, depending on the specific burn severity metric analysed and the approach used (i.e. composite *v.* paired; Fig. 2 and Table 2). The quality of model fits relating CBI to severity metrics calculated from paired images and mean compositing were not meaningfully different (differences in $R^2 = \pm \leq 0.05$ between paired and composited for all severity metrics; Fig. 2 and Table 2). Paired images generally had slightly higher correspondence to field data, and error (RMSE) and bias (MAE) were also marginally higher when mean composited metrics were used (Table 2; Fig. A1).

Individual pixel values of severity metrics were highly correlated between paired and mean composited maps (dNBR CV $r = 0.90$; RdNBR CV $r = 0.87$; RBR CV $r = 0.91$; $P < 0.001$ for all tests). Cross-validated burn severity threshold values derived from models using paired and composited imagery were all significantly different from one another (Fig. 3 and Table A1 (Appendix 1); no overlap in 95% confidence intervals).

Burn severity maps produced using mean compositing in GEE increased the number of pixels with data by 0 to 11.3%, with an average per-fire gain in mapped area of 4.2% and a total gain of 8.9% of pixels or 123 526 ha across the 11 fires used for validation, as compared with the burn severity maps produced

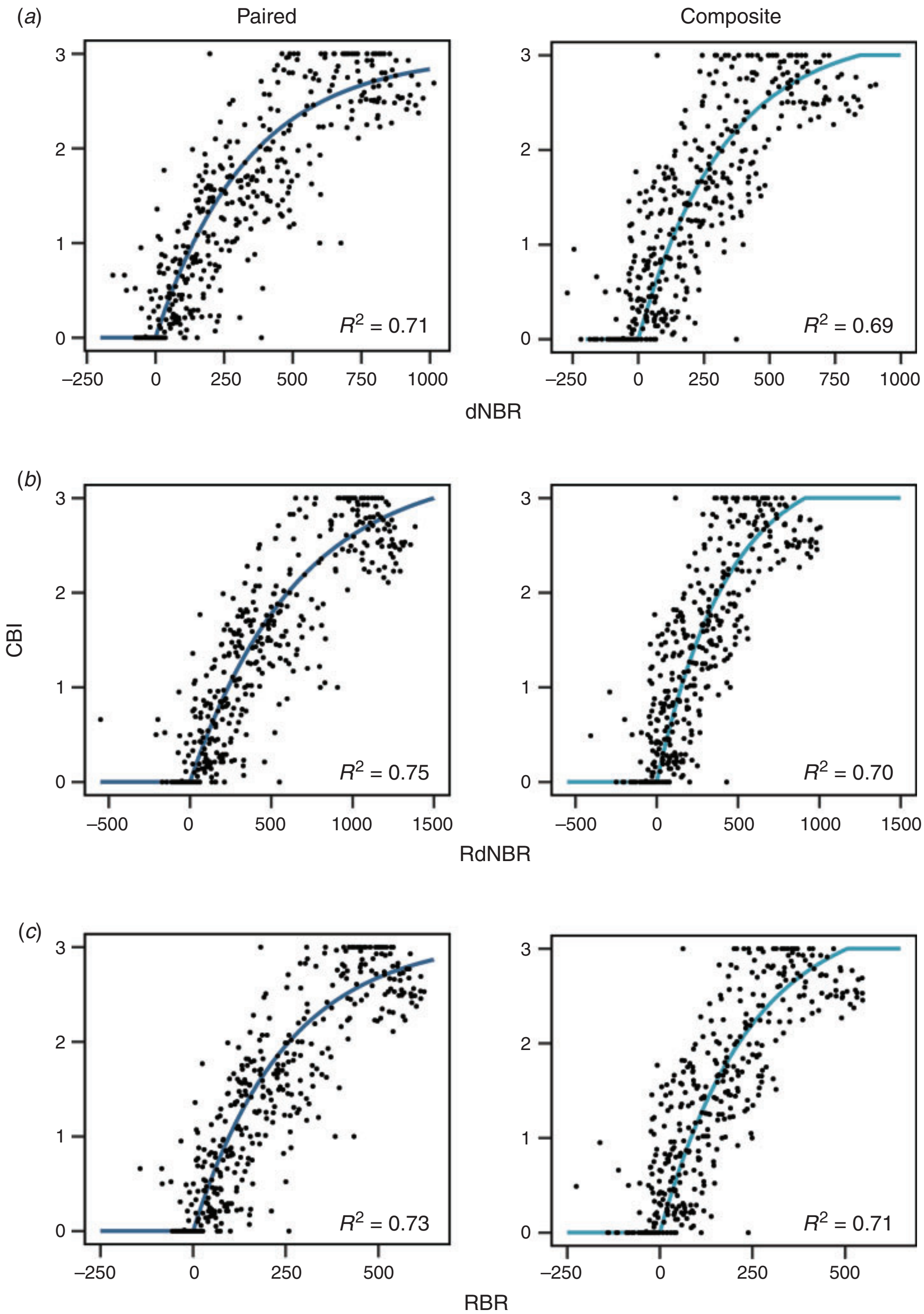


**Fig. 2.** Fit and form of saturated growth models of Composite Burn Index (CBI) as a function of remotely sensed burn severity metrics of the differenced Normalized Burn Ratio (dNBR) (*a*); the Relativised differenced Normalized Burn Ratio (RdNBR) (*b*); and Relativized Burn Ratio (RBR) (*c*). The left column displays models fitted with severity metrics calculated from paired individual pre-fire and post-fire scenes selected by an analyst, whereas the right column displays models fitted with severity metrics calculated from mean-compositing of pixels.

using paired images. Most of pixels within the 11 sampled fires had both pre-fire and post-fire mean composite imagery from the years immediately before and after the fire (between 95.7 and 100% of pixels per fire; 98.5% of all pixels). Only 0.54% of all pixels used either pre-fire or post-fire imagery from 2 years before or after the fire. The final 0.96% of pixels used pre-fire imagery from more than 2 years before the fire or both the pre-fire and post-fire imagery were from 2 years before and after the fire.

Because the differences between the validation statistics of the paired and mean composite approach were minimal and the mean composite approach yielded more spatially comprehensive maps, we produced a complete burn severity atlas using

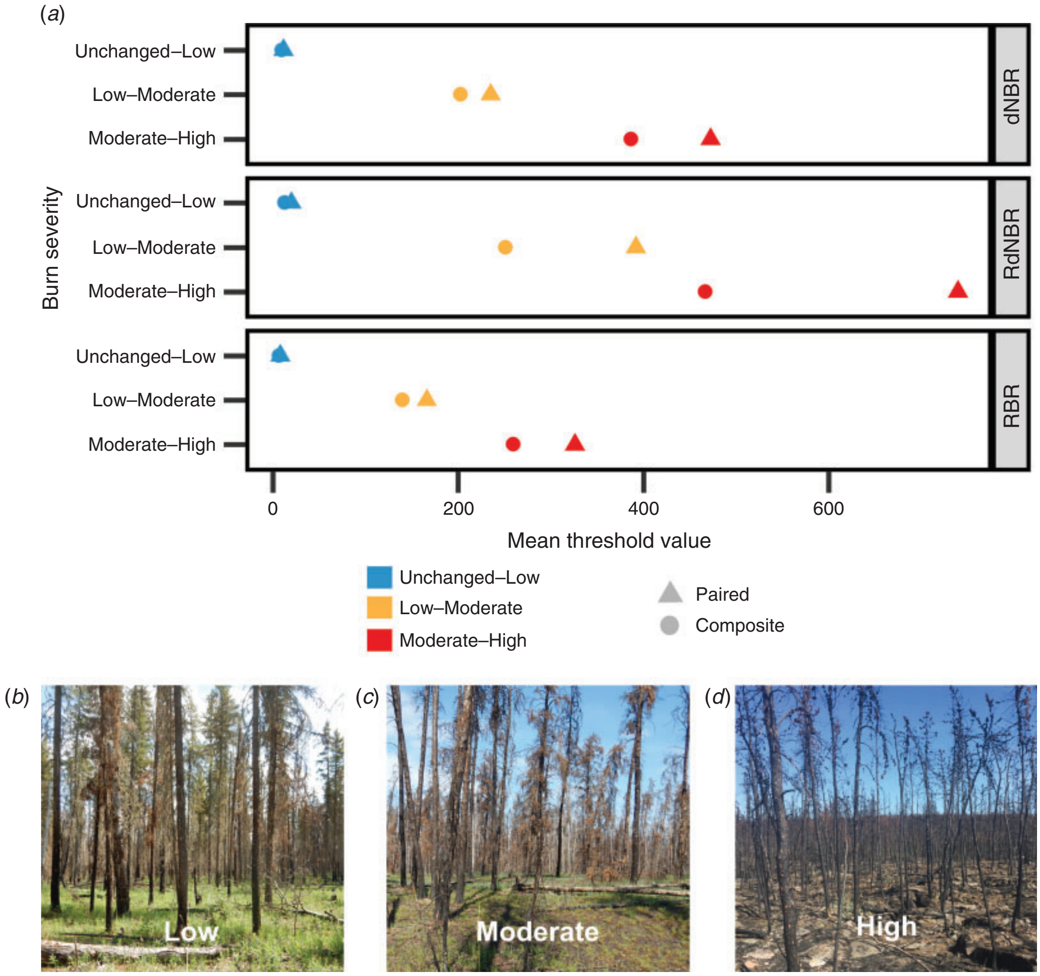


**Fig. 3.** (*a*) Mean values for burn severity class thresholds (unchanged–low Composite Burn Index (CBI) = 0.1; low–moderate CBI = 1.5; and moderate–high CBI = 2.25) from paired (triangles) and composite (light circles) imagery. Threshold estimates for remotely sensed severity indices were produced using cross-validation (CV) with models fitted using 80% of fires with 1000 repeats. We report mean threshold values and 95% confidence intervals calculated using the adjusted bootstrap percentile (BCa) method with 1000 resamples reported in Table A1 (Appendix 1) Photographs of (*b*) low-severity, (*c*) moderate-severity, and (*d*) high-severity burned jack pine (*Pinus banksiana*) forests are presented to represent differences between burn severity classes identified from CBI models (dNBR, Normalized Burn Ratio; RdNBR, Relativised differenced Normalized Burn Ratio; RBR, Relativized Burn Ratio).

mean compositing for all 796 sampled fires in GEE. The code used for this purpose is available here: http://tidy.ws/4nkdMU. Within the atlas, some fire events occurred near one another (<180 m between mapped fire edges) in close succession. A total of 157 fires had some overlap with a previous fire event that had occurred ≤5 years before the fire of interest. Of these fires with some buffer overlap, only 15 had >40% of the total buffer area inside a prior burn. These 15 fires are identified in the atlas data, and make up ~0.6% of the total area of the atlas.

## Discussion

Remotely sensed burn severity maps produced using semi-automated mean-compositing and analyst-selected paired images both represented field measurements of burn severity very well (Table 2). Models relating CBI and remotely sensed burn severity can be used to convert remotely sensed metrics into maps of CBI, in order to better represent severity on the ground (Parks *et al.* 2019). Although we produced models relating CBI to remotely sensed burn severity, we did not convert the mean-composited burn severity atlas into modelled CBI values. We took this approach in order to present a simple method and resulting atlas that users could then adapt for their own uses (e.g. build their own severity models and employ severity metrics other than CBI). Those wishing to use this atlas to map CBI can create thresholded severity maps using the classes reported here (Table A1). The significant difference between severity class thresholds derived from models predicting CBI from paired images and mean composited imagery (Fig. 3) highlights that the two datasets have significantly different relationships to CBI and thresholds identified in research using one data source cannot be applied to the other without confirming that the relationship with field observations is similar. The generally lower values and smaller range in the mean composited datasets is likely due to the effect of averaging in removing and reducing extreme reflectance values that remain in the single-date paired imagery. This, along with the use of an unburned offset, translated to much lower thresholds for classifying continuous severity imagery, relative to those reported in other regions (e.g. Key and Benson 2006; Kolden *et al.* 2012; Meigs and Krawchuk 2018), as well as in boreal forests (Hall *et al.* 2008). These differences in threshold values may also relate to the fact that thresholds used by others have been developed to differentiate between the prevalence of live and dead trees (e.g. Meigs and Krawchuk 2018) rather than truly unburned areas.

We found no meaningful difference in the quality of burn severity maps produced using mean-composited and paired images; however, mean-composited maps had slightly lower pseudo-$R^2$ values and slightly higher model error when used to predict CBI. The marginally lower correspondence of the composited imagery severity metrics to CBI may indicate that analyst selection of images may allow for a refined choice of imagery, accounting for image quality issues not captured in the automated Landsat image quality masks used to exclude clouded and shadowed pixels from this analysis. Although there was no substantial difference in the quality of the modelled fit between CBI and the two methods of deriving burn severity maps in this study, others have observed an improvement in the correspondence to field data using mean compositing (Parks *et al.* 2018). The different response observed here may be due to the smaller number of fires (11 *v.* 18) and field sites analysed in the present study, or known challenges to mapping fire severity with remote sensing in northern latitudes and mountainous areas (including high cloud cover, low insolation angles and aspect effects on reflectance (Verbyla *et al.* 2008; Hermosilla *et al.* 2016)). Furthermore, the sample of fires examined by Parks *et al.* (2018) were taken from western US forests, which may be a more regionally homogeneous group in composition and structure (known to affect fire severity metrics (Harvey *et al.* 2019)), as compared with the combination of boreal and montane forests used for the present study. It is likely that including additional stratification of plots by vegetation (fuel) types, or other ecological drivers that may affect severity (e.g. topography, regional moisture) in multivariate models would improve the predictive power of the remotely sensed severity metrics and reduce the error associated with the composited imagery by explaining additional variability in severity (e.g. Whitman *et al.* 2018*a*; Harvey *et al.* 2019; Parks *et al.* 2019). Nonetheless, the bivariate models provide a good representation of CBI without this modification (Table 2).

Other researchers have used segmentation algorithms to smooth spectral reflectance values used for atlases of fire impacts spanning multiple years (Reilly *et al.* 2017). Our findings that the mean composited severity maps corresponded well to field data from a diverse group of fires from several years, along with other research demonstrating that dNBR and related severity metrics are largely insensitive to which Landsat sensor, or combination of sensors, is used (Chen *et al.* 2020) suggest that such smoothing may not be necessary.

Using the mean compositing approach led to a gain in the total area mapped with valid burn severity values within sampled fires owing to the inclusion of cloud-free pixels from multiple days within the growing season, and, less often, from other years (i.e. beyond the standard 1 year pre and post imagery selection window). This is in contrast to the single-date paired images that were partially obscured by smoke or clouds, and in some cases, did not cover the total extent of the fire perimeter, leading to pixels having no valid fire severity values. Mean compositing also overcame the limitations of Landsat 7 ETM+ imagery from the era of the Scan Line Corrector (SLC) failure, by filling SLC-off gaps with composites from other clear images, while retaining those pixels with valid imagery. Fires that occurred in the SLC failure era may have slightly fewer clear pixels available for compositing for this reason. Although this method fills the extensive SLC-off gaps with no data, the SLC-off gap areas may have slightly less consistent pixel values due to a relative lack of clear imagery. Additionally, the region studied for our purposes has very large fires (e.g. >50 000 ha). These fires often extend across multiple Landsat scenes, requiring an analyst to mosaic multiple images, or to leave out a portion of a fire perimeter if clear images from a similar date are not available. Mean compositing requires no mosaicing of rasters, saving analysts time and using all possible clear pixels for mapping purposes, regardless of whether they fall into the same 'tile'. We found that mean compositing increased the number of pixels with remotely sensed severity data by 8.9% in the sampled fires. Such gains represent a small proportion of burned area, but are significant in terms of land area. For example, considering the entire atlas of 796 fires (7 039 147 ha of area within fire perimeters), an 8.9% gain in mappable pixels (30-m resolution) equates to a 627 376 ha increase in area with fire severity data that would have been obscured by clouds or shadows with paired-image maps.

Mean compositing and longer image selection windows come with some trade-offs, and may not be appropriate in all ecosystems. For example, in grasslands, swamps and any forests that revegetate rapidly after fire, this method and a longer image selection window (≥2 years after a fire) would likely obscure the signal from vegetation mortality and biomass loss, leading to underestimations of both burn severity and area burned (Picotte and Robertson 2011; Lu *et al.* 2016). We limited post-fire imagery to a maximum of 2 years post fire, well below the ~5 years necessary in slow-growing cold and temperate forests such as these to recover from disturbance and show altered spatial patterns in NBR time series (Pickell *et al.* 2015; Kansas *et al.* 2016). In forests and ecosystems with slow post-fire recoveries, such as those studied here, the gain in area that can be mapped without being obscured by cloud and smoke (both common summer occurrences in the north and in mountainous regions) by using mean compositing and extended image selection windows is valuable and does not come at the expense of data quality (Table 2).

### *Applications*

This effort confirms that the creation of a comprehensive burn severity atlas for a large region can be automated, reducing the need for analyst decision-making and time. The complete Alberta and national parks burn severity atlas is available for download upon request. Examples of RBR burn severity maps for several

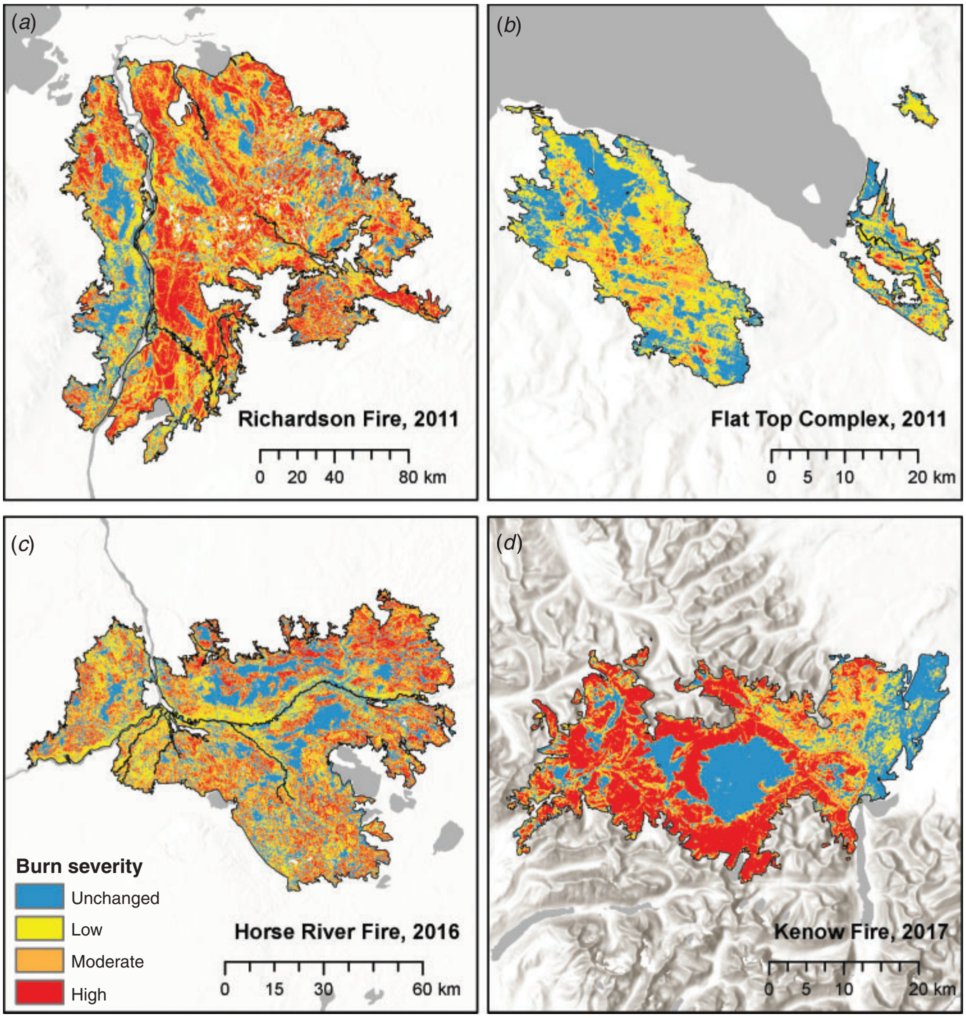


**Fig. 4.** Example remotely sensed burn severity maps derived from mean compositing of pixels in Google Earth Engine for selected fires of interest. Burn severity was derived from classified Relativized Burn Ratio (RBR) maps, with thresholds for unchanged, low, moderate, and high fire severity reported in Table A1 (Appendix 1). Dark grey areas indicate water. Mapped fires are: (*a*) the Richardson Fire (north-eastern AB); (*b*) the Flat Top Complex (Slave Lake, AB); (*c*) the Horse River Fire (Fort McMurray, AB); and (*d*) the Kenow Fire (Waterton Lakes National Park, AB).

notable fires in the study area and period (1985–2018; Fig. 1) are shown in Fig. 4. The Richardson fire (2011) is a large wildfire that burned in a boreal forest wilderness area, across the borders of three fire management agencies in Wood Buffalo National Park, AB, and into Saskatchewan (SK). The Flat Top complex (2011) notoriously destroyed a substantial part of the town of Slave Lake, AB. Similarly, the Horse River fire (2016) burned homes in several neighbourhoods of Fort McMurray, leading to the largest insurable loss in Canadian history (Insurance Bureau of Canada 2019). Most recently, the Kenow fire (2017) burned much of the land base of Waterton Lakes National Park at very high severity (Fig. 4). Burn severity is highly variable between and within fires, contributing to diverse responses in the post-fire ecology of trees and plants (Harvey *et al.* 2016; Abatzoglou *et al.* 2017; Whitman *et al.* 2018*a*). Atlases such as this are a desirable product for managers and researchers alike and can be used to plan field-based interventions and studies, as well as conducting large-scale spatial analyses. Such atlases can be used to examine trends in burn severity over time (Picotte *et al.* 2016; Stevens *et al.* 2016) and between repeated fires (Parks *et al.* 2014*b*; Stevens-Rumann *et al.* 2016), to examine how burn severity and other landscape forest disturbances interact (Harvey *et al.* 2013; Meigs *et al.* 2016), or to map unburned residuals (Kolden *et al.* 2012; Meigs *et al.* 2020), offering insight into fire ecology, fire behaviour and post-fire forest regeneration in regions where burn severity atlases were previously not available.

Although we successfully mapped all large fires during the defined period in the study area, we encountered several challenges that required special consideration. Wildfires regularly cross jurisdictional or managerial boundaries, and yet perimeters collected by different fire agencies may be inconsistent and require substantial processing (e.g. combining, substituting or redelineating cross-boundary fire perimeters). Furthermore, fires may burn together through the course of a

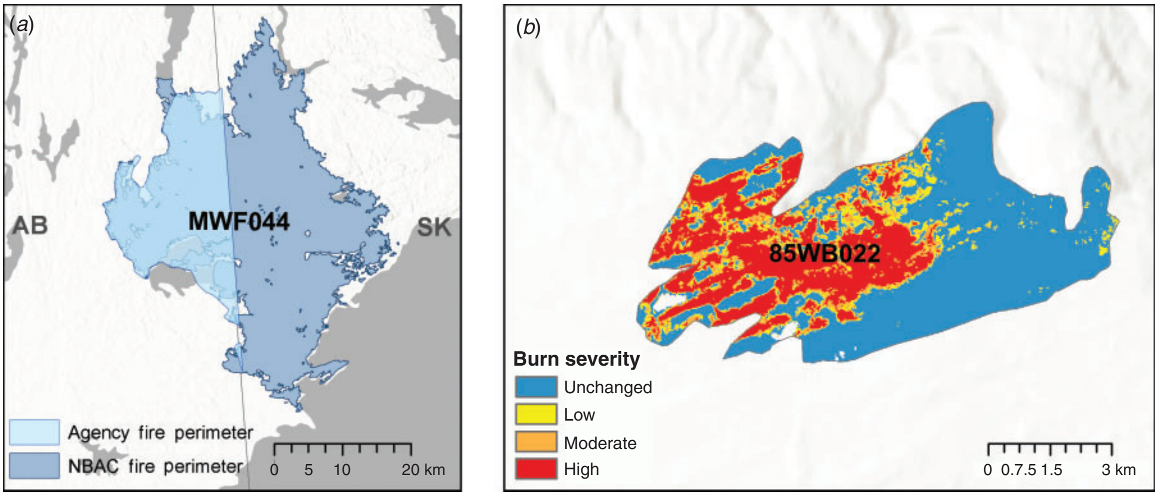


**Fig. 5.** Fire perimeters representing examples of processing challenges faced when mapping burn severity using Google Earth Engine (GEE). Fire perimeter maps that produce errors or inaccurate severity maps include: (*a*) fire perimeters that stop at borders between management agencies, and (*b*) poorly mapped fire perimeters that include large unburned areas outside the actual fire perimeter and exclude some burned areas, with no alternative perimeter map source (NBAC, National Burned Area Composite).

fire season but remain mapped as separate incidents. If multiple adjacent perimeters are used to delineate a spatially continuous or contiguous burned area, burned areas outside mapped perimeters may be included in the buffer used for calculating the offset, and the offset value will be incorrectly calculated. In the dataset developed here, we replaced such perimeters with those provided by the NBAC (Fig. 5*a*; Hall *et al.* 2020). Users with similar problems who cannot combine perimeters may opt not to normalise burn severity with an offset value.

Refined fire perimeters may be available from alternative sources, but in many cases, old wildfires (early in the satellite record) or smaller fires are only available from coarse data sources, such as helicopter-flown global positioning system (GPS) track or hand-mapped perimeters derived from lower-resolution or old imagery. In those cases, the resulting severity raster may be missing burned areas and include large unburned areas (Fig. 5*b*). This issue cannot be easily corrected without redelineating the perimeter, either through digitising by an analyst or through remote sensing processes and algorithms, such as multi-acquisition fire mapping systems (*MAFiMS*) software (Hall *et al.* 2020). Users who wish to apply this method but who are limited by fire perimeter quality or availability could consider buffering poor-quality perimeters, hotspots or low-resolution satellite burned area products before producing severity maps in order to include burned areas that may have been missed. Alternatively, users could define a large area of interest around an approximate fire location or for an entire atlas study area and use that region to produce annual severity maps that would include unburned areas in addition to burned areas. Both of these approaches would introduce additional unburned areas outside true fire perimeters. Users could refine these annual grids by post-processing to delineate individual fire perimeters in order to develop a perimeter database, which could then be used to process severity maps for individual fires, if desired. Simply put, the burn severity metrics could themselves be used to identify accurate fire boundaries.

## Conclusion

Producing burn severity maps using mean compositing of pixels in cloud computing platforms such as GEE presents an excellent opportunity for managers and researchers to develop temporally and spatially extensive fire severity atlases, comparable with that provided in the United States through the MTBS program. The Landsat archive's global coverage and extensive history (>30 years) make this exercise easily achievable and possible for broad application in other countries, provinces or states and regions, and in cross-jurisdictional areas. In western Canada, semi-automated burn severity metrics produced using mean compositing and paired images produced by an analyst represent field measurements of burn severity equally well, and are highly correlated with one another. The savings of time and the modest increases in the proportion of a fire perimeter with meaningful severity data suggest that mean compositing of severity metrics in a cloud computing platform is ideal for applications in jurisdictions with small staff levels and budgets, as well as in areas with less frequent sunny and clear days. The code used to develop the atlas described here is available for the use and adaptation by any such organisation or researcher wishing to produce their own burn severity atlas.

## Conflicts of interest

The authors declare no conflicts of interest.

## Acknowledgements

Field data used to validate remotely sensed products were collected for research funded in part by the Natural Sciences and Engineering Research Council of Canada (funding reference no. CGSD3-471480-2015) and the Government of the Northwest Territories. We thank Kiera Macauley and Parks Canada for providing additional field data used in the validation of this atlas. We also acknowledge and thank the external reviewers of this work, who provided suggestions and insight that substantially improved the quality of this paper.

## References

Abatzoglou JT, Kolden CA, Williams AP, Lutz JA, Smith AMS (2017) Climatic influences on interannual variability in regional burn severity across western US forests. *International Journal of Wildland Fire* **26**, 269–275. doi:10.1071/WF16165

Boucher J, Beaudoin A, Hébert C, Guindon L, Bauce É (2017) Assessing the potential of the differenced Normalized Burn Ratio (dNBR) for estimating burn severity in eastern Canadian boreal forests. *International Journal of Wildland Fire* **26**, 32–45. doi:10.1071/WF15122

Chen D, Loboda T, Hall JV (2020) A systematic evaluation of image selection process on remote sensing-based burn severity indices in North American boreal forest and tundra ecosystems. *ISPRS Journal of Photogrammetry and Remote Sensing* **159**, 63–77. doi:10.1016/J.ISPRSJPRS.2019.11.011

De Santis A, Chuvieco E (2009) GeoCBI: a modified version of the Composite Burn Index for the initial assessment of the short-term burn severity from remotely sensed data. *Remote Sensing of Environment* **113**, 554–562. doi:10.1016/J.RSE.2008.10.011

DeLong C, Meidinger D (2003) Ecological variability of high-elevation forests in central British Columbia. *Forestry Chronicle* **79**, 259–262. doi:10.5558/TFC79259-2

Ecological Stratification Working Group (ESWG) (1995) 'A national ecological framework for Canada.' (Agriculture and Agri-Food Canada: Ottawa, ON, Canada).

Eidenshink J, Schwind B, Brewer K, Zhu Z-L, Quayle B, Howard S (2007) A project for monitoring trends in burn severity. *Fire Ecology* **3**, 3–21. doi:10.4996/FIREECOLOGY.0301003

Forestry Canada Fire Danger Group (1992) Development and structure of the Canadian Forest Fire Behavior Prediction System. Forestry Canada, Information Report ST-X-3 (Ottawa, ON, Canada).

French NHF, Kasischke ES, Hall RJ, Murphy KA, Verbyla DL, Hoy EE, Allen JL (2008) Using Landsat data to assess fire and burn severity in the North American boreal forest region: an overview and summary of results. *International Journal of Wildland Fire* **17**, 443–463. doi:10.1071/WF08007

Greenwell BM, Schubert Kabban CM (2014) investr: an *R* package for inverse estimation. *The R Journal* **6**, 90–100. doi:10.32614/RJ-2014-009

Hall RJ, Freeburn JT, De Groot WJ, Pritchard JM, Lynham TJ, Landry R (2008) Remote sensing of burn severity: experience from western Canada boreal fires. *International Journal of Wildland Fire* **17**, 476–489. doi:10.1071/WF08013

Hall RJ, Skakun RS, Metsaranta JM, Landry R, Fraser RH, Raymond D, Gartrell M, Decker V, Little J (2020) Generating annual estimates of forest fire disturbance in Canada: The National Burned Area Composite. *International Journal of Wildland Fire* . doi:10.1071/WF19201

Hanes CC, Wang X, Jain P, Parisien M, Little JM (2019) Fire regime changes in Canada over the last half century. *Canadian Journal of Forest Research* **49**, 256–269. doi:10.1139/CJFR-2018-0293

Harvey BJ, Donato DC, Romme WH, Turner MG (2013) Influence of recent bark beetle outbreak on fire severity and post-fire tree regeneration in montane Douglas-fir forests. *Ecology* **94**, 2475–2486. doi:10.1890/13-0188.1

Harvey BJ, Donato DC, Turner MG (2016) Drivers and trends in landscape patterns of stand-replacing fire in forests of the US northern Rocky Mountains (1984–2010). *Landscape Ecology* **31**, 2367–2383. doi:10.1007/S10980-016-0408-4

Harvey BJ, Andrus RA, Anderson SC (2019) Incorporating biophysical gradients and uncertainty into burn severity maps in a temperate fire-prone forested region. *Ecosphere* **10**, e02600. doi:10.1002/ECS2.2600

Hermosilla T, Wulder MA, White JC, Coops NC, Hobart GW, Campbell LB (2016) Mass data processing of time series Landsat imagery: pixels to data products for forest monitoring. *International Journal of Digital Earth* **9**, 1035–1054. doi:10.1080/17538947.2016.1187673

Insurance Bureau of Canada (2019) Three years later: what you need to know. Available at http://assets.ibc.ca/Documents/Disaster/Three_Years Later.pdf [Verified 5 August 2020]

Kansas J, Vargas J, Skatter HG, Balicki B, McCullum K (2016) Using Landsat imagery to backcast fire and post-fire residuals in the Boreal Shield of Saskatchewan: implications for woodland caribou management. *International Journal of Wildland Fire* **25**, 597–697. doi:10.1071/WF15170

Key CH, Benson NC (2006) Landscape assessment (LA): sampling and analysis methods. USDA Forest Service, Rocky Mountain Research Station Research station, General Technical Report RMRS-GTR-164-CD, pp. LA-1–55. (Fort Collins, CO, USA)

Kolden CA, Lutz JA, Key CH, Kane JT, van Wagtendonk JW (2012) Mapped versus actual burned area within wildfire perimeters: characterizing the unburned. *Forest Ecology and Management* **286**, 38–47. doi:10.1016/J.FORECO.2012.08.020

Krawchuk MA, Moritz MA, Parisien M-A, Van Dorn J, Hayhoe K (2009) Global pyrogeography: the current and future distribution of wildfire. *PLoS One* **4**, e5102. doi:10.1371/JOURNAL.PONE.0005102

Lu B, He Y, Tong A (2016) Evaluation of spectral indices for estimating burn severity in semiarid grasslands. *International Journal of Wildland Fire* **25**, 147–157. doi:10.1071/WF15098

Masek JG, Vermote EF, Saleous NE, Wolfe R, Hall FG, Huemmrich KF, Gao F, Kutler J, Lim T-K (2006) A Landsat surface reflectance dataset for North America, 1990–2000. *IEEE Geoscience and Remote Sensing Letters* **3**, 68–72. doi:10.1109/LGRS.2005.857030

Meigs GW, Krawchuk MA (2018) Composition and structure of forest fire refugia: what are ecosystem legacies across burned landscapes? *Forests* **9**, 243. doi:10.3390/F9050243

Meigs GW, Zald HS, Campbell JL, Keeton WS, Kennedy RE (2016) Do insect outbreaks reduce the severity of subsequent forest fires? *Environmental Research Letters* **11**, 045008. doi:10.1088/1748-9326/11/4/045008

Meigs GW, Dunn CJ, Parks SA, Krawchuk MA (2020) Influence of topography and fuels on fire refugia probability under varying fire weather in forests of the US Pacific Northwest. *Canadian Journal of Forest Research* **50**, 636–647. doi:10.1139/CJFR-2019-0406

Miller JD, Thode AE (2007) Quantifying burn severity in a heterogeneous landscape with a relative version of the delta Normalized Burn Ratio (dNBR). *Remote Sensing of Environment* **109**, 66–80. doi:10.1016/J.RSE.2006.12.006

Morgan P, Keane RE, Dillon GK, Jain TB, Hudak AT, Karau EC, Sikkink PG, Holden ZA, Strand EK (2014) Challenges of assessing fire and burn severity using field measures, remote sensing and modelling. *International Journal of Wildland Fire* **23**, 1045–1060. doi:10.1071/WF13058

Natural Resources Canada (2011) Canadian Digital Elevation Model, 1945 – 2011. Canada Centre for Mapping and Earth Observation. Ottawa, ON. Available at https://open.canada.ca/data/en/dataset/7f245e4d-76c2-4caa-951a-45d1d2051333 [Verified 5 August 2020]

Natural Resources Canada (2019) Canadian national fire database – agency fire data. (Edmonton, AB, Canada) Available at https://cwfis.cfs.nrcan.gc.ca/ha/nfdb [Verified 5 August 2020]

Parks SA, Dillon GK, Miller C (2014*a*) A new metric for quantifying burn severity: the Relativized Burn Ratio. *Remote Sensing* **6**, 1827–1844. doi:10.3390/RS6031827

Parks SA, Miller C, Nelson CR, Holden ZA (2014*b*) Previous fires moderate burn severity of subsequent wildland fires in two large western US wilderness areas. *Ecosystems* **17**, 29–42. doi:10.1007/S10021-013-9704-X

Parks SA, Holsinger LM, Voss MA, Loehman RA, Robinson NP (2018) Mean composite fire severity metrics computed with Google Earth Engine offer improved accuracy and expanded mapping potential. *Remote Sensing* **10**, 879. doi:10.3390/RS10060879

Parks SA, Holsinger LM, Koontz MJ, Collins L, Whitman E, Parisien M-A, Loehman RA,, Barnes JL, Bourdon JF, Boucher J, Boucher Y, Caprio AC, Collingwood A, Hall RJ, Park J, Saperstein LB, Smetanka C, Smith RJ, Soverel N (2019) Giving ecological meaning to satellite-derived fire severity metrics across North American forests. *Remote Sensing* **11**, 1735. doi:10.3390/RS11141735

Pickell PD, Hermosilla T, Frazier RJ, Coops NC, Wulder MA (2015) Forest recovery trends derived from Landsat time series for North America boreal forests. *International Journal of Remote Sensing* **37**, 138–149. doi:10.1080/2150704X.2015.1126375

Picotte JJ, Robertson K (2011) Timing constraints on remote sensing of wildland fire burned area in the south-eastern US. *Remote Sensing* **3**, 1680–1690. doi:10.3390/RS3081680

Picotte JJ, Peterson B, Meier G, Howard SM (2016) 1984–2010 trends in fire burn severity and area for the conterminous US. *International Journal of Wildland Fire* **25**, 413–420. doi:10.1071/WF15039

Reilly MJ, Dunn CJ, Meigs GW, Spies TA, Kennedy RE, Bailey JD, Briggs K (2017) Contemporary patterns of fire extent and severity in forests of the Pacific Northwest, USA (1985 – 2010). *Ecosphere* **8**, e01695. doi:10.1002/ECS2.1695

Rogeau M-P, Pengelly I, Fortin M-J (2004) Using topography to model and monitor fire cycles in Banff National Park. In 'Proceedings of the 22nd Tall Timbers fire ecology conference: fire in temperate, boreal, and montane ecosystems' (Eds RT Engstrom, KEM Galley, WJ de Groot) pp. 55–69. (Tall Timbers Research Station: Tallahasse, FL, USA)

San-Miguel I, Andison DW, Coops NC, Rickbeil GJM (2016) Predicting post-fire canopy mortality in the boreal forest from dNBR derived from time series of Landsat data. *International Journal of Wildland Fire* **25**, 762–774. doi:10.1071/WF15226

San-Miguel I, Andison DW, Coops NC (2019) Quantifying local fire regimes using the Landsat data-archive: a conceptual framework to derive detailed fire pattern metrics from pixel-level information. *International Journal of Digital Earth* **12**, 544–565. doi:10.1080/17538947.2018.1464072

Schoennagel T, Smithwick EAH, Turner MG (2008) Landscape heterogeneity following large fires: insights from Yellowstone National Park, USA. *International Journal of Wildland Fire* **17**, 742–753. doi:10.1071/WF07146

Skowronski NS, Gallagher MR, Warner TA (2020) Decomposing the interactions between fire severity and canopy fuel structure using multitemporal, active, and passive remote sensing approaches. *Fire* **3**, 7. doi:10.3390/FIRE3010007

Soverel NO, Perrakis DDB, Coops NC (2010) Estimating burn severity from Landsat dNBR and RdNBR indices across western Canada. *Remote Sensing of Environment* **114**, 1896–1909. doi:10.1016/J.RSE.2010.03.013

Stevens JT, Collins BM, Miller JD, North MP, Stephens SL (2016) Changing spatial patterns of stand-replacing fire in California conifer forests. *Forest Ecology and Management* **406**, 28–36. doi:10.1016/J.FORECO.2017.08.051

Stevens-Rumann CS, Prichard SJ, Strand EK, Morgan P (2016) Prior wildfires influence burn severity of subsequent large fires. *Canadian Journal of Forest Research* **46**, 1375–1385. doi:10.1139/CJFR-2016-0185

Stocks BJ, Mason JA, Todd JB, Bosch EM, Wotton BM, Amiro BD, Flannigan MD, Hirsch KG, Logan KA, Martell DL, Skinner WR (2002) Large forest fires in Canada, 1959–1997. *Journal of Geophysical Research* **107**, FFR 5–1–FFR 5–12. doi:10.1029/2001JD000484

Turner MG, Romme WH, Gardner RH (1999) Pre-fire heterogeneity, fire severity, and early post-fire plant reestablishment in subalpine forests of Yellowstone National Park, Wyoming. *International Journal of Wildland Fire* **9**, 21–36. doi:10.1071/WF99003

Tymstra C, Wang D, Rogeau M-P (2005) Alberta wildfire regime analysis. Alberta Department of Sustainable Resource Development, Wildfire Science and Technology Report PFFC-01–05. (Edmonton, AB, Canada)

US Geological Survey, USDA Forest Service, USDI (2019) MTBS: project overview. Available at https://www.mtbs.gov/index.php/project-overview [Verified 5 August 2020]

Verbyla DL, Kasischke ES, Hoy EE (2008) Seasonal and topographic effects on estimating fire severity from Landsat TM/ETM+ data. *International Journal of Wildland Fire* **17**, 527–534. doi:10.1071/WF08038

Vermote E, Justice C, Claverie M, Franch B (2016) Preliminary analysis of the performance of the Landsat8/OLI land surface reflectance product. *Remote Sensing of Environment* **185**, 46–56. doi:10.1016/J.RSE.2016.04.008

White JC, Wulder MA, Hobart GW, Luther JE, Hermosilla T, Griffiths P, Coops NC, Hall RJ, Hostert P, Dyk A, Guindon L, Coops NC, Hall RJ, Hostert P, Dyk A, Guindon L (2014) Pixel-based image compositing for large-area dense time series applications and science. *Canadian Journal of Remote Sensing* **40**, 192–212. doi:10.1080/07038992.2014.945827

Whitman E, Batllori E, Parisien M-A, Miller C, Coop JD, Krawchuk MA, Chong GW, Haire SL (2015) The climate space of fire regimes in north-western North America. *Journal of Biogeography* **42**, 1736–1749. doi:10.1111/JBI.12533

Whitman E, Parisien M-A, Thompson DK, Hall RJ, Skakun RS, Flannigan MD (2018*a*) Variability and drivers of burn severity in the north-western Canadian boreal forest. *Ecosphere* **9**, e02128. doi:10.1002/ECS2.2128

Whitman E, Parisien MA, Thompson DK, Flannigan MD (2018*b*) Topoedaphic and forest controls on post-fire vegetation assemblies are modified by fire history and burn severity in the north-western Canadian boreal forest. *Forests* **9**, 151. doi:10.3390/F9030151

Wierzchowski J, Heathcott M, Flannigan MD (2002) Lightning and lightning fire, Central Cordillera, Canada. *International Journal of Wildland Fire* **11**, 41–52. doi:10.1071/WF01048

Wilson DJ (2019) The harmonic mean *p*-value for combining dependent tests. *Proceedings of the National Academy of Sciences of the United States of America* **116**, 1195–1200. doi:10.1073/PNAS.1814092116

## Appendix 1

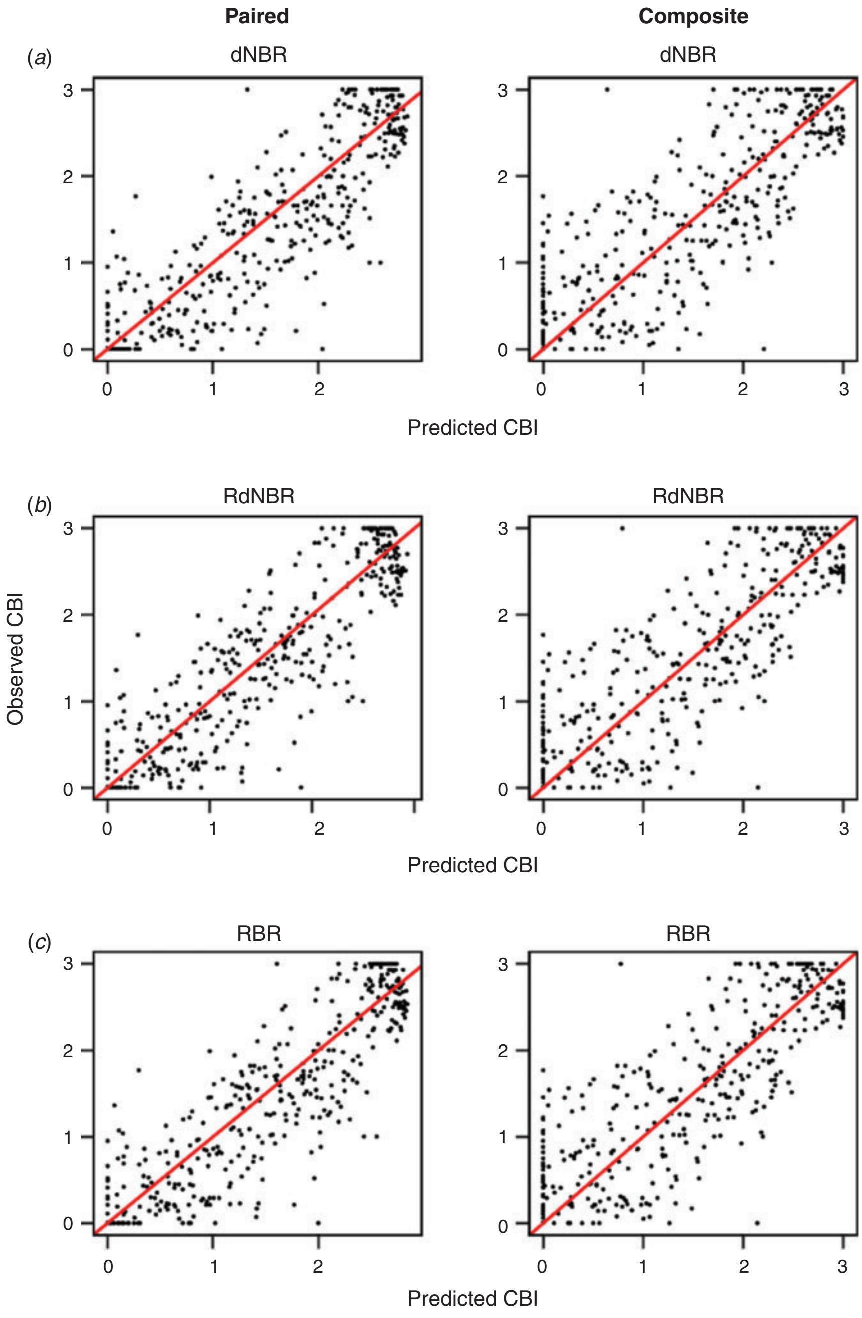


**Fig. A1.** Correspondence between observed (*y*-axis) and predicted (*x*-axis) values from generalised linear models of Composite Burn Index (CBI) as a function of remotely sensed burn severity metrics of the differenced Normalized Burn Ratio (dNBR) (*a*); the Relativized differenced Normalised Burn Ratio (RdNBR) (*b*); and Relativised Burn Ratio (RBR) (*c*). The left column displays model fits from severity metrics calculated from paired individual pre-fire and post-fire scenes selected by an analyst, whereas the right column displays model fits from mean-compositing of pixels.

**Table A1. Modelled burn severity thresholds used to classify burn severity values for all ($n = 11$) sampled fires**

Threshold values are predicted using inverse estimation from non-linear least-squares saturated growth models predicting CBI from remotely sensed severity metric values, and represent the range corresponding to unchanged (0–0.5), low- (>0.5–1.5), moderate- (>1.5–2.25), and high- (>2.25) severity CBI. We calculated bootstrapped 95% confidence intervals (CIs) for mean threshold values using the adjusted bootstrap percentile (BCa) method with 1000 resamples

| Severity metric | Unchanged–low mean threshold (95% CI) | Low–moderate mean threshold (95% CI) | Moderate–high mean threshold (95% CI) |
|---|---|---|---|
| $dNBR_{paired}$ | 11.46 (11.44–11.48) | 234.94 (234.40–235.50) | 472.47 (470.50–474.10) |
| $dNBR_{composite}$ | 10.24 (10.22–10.26) | 202.78 (202.40–202.78) | 386.95 (385.60–388.30) |
| $RdNBR_{paired}$ | 19.94 (19.85–20.04) | 391.78 (390.00–393.30) | 739.40 (737.10–741.90) |
| $RdNBR_{composite}$ | 12.94 (12.90–12.98) | 251.18 (250.50–251.90) | 466.91 (465.40–468.50) |
| $RBR_{paired}$ | 8.22 (8.21–8.24) | 166.09 (165.70–166.40) | 325.81 (324.80–326.90) |
| $RBR_{composite}$ | 7.22 (7.20–7.24) | 140.01 (139.60–140.40) | 259.94 (259.00–260.90) |